

Zili Wu

List of Publications by Year in descending order

Source: <https://exaly.com/author-pdf/4534766/publications.pdf>

Version: 2024-02-01

253
papers

16,714
citations

14614

66
h-index

18075

120
g-index

267
all docs

267
docs citations

267
times ranked

18325
citing authors

#	ARTICLE	IF	CITATIONS
1	Manipulating Copper Dispersion on Ceria for Enhanced Catalysis: A Nanocrystal-Based Atom-Trapping Strategy. <i>Advanced Science</i> , 2022, 9, e2104749.	5.6	16
2	Ammonia synthesis on BaTiO _{2.5} H _{0.5} : computational insights into the role of hydrides. <i>Physical Chemistry Chemical Physics</i> , 2022, 24, 1496-1502.	1.3	4
3	Can Li: A Career in Catalysis. <i>ACS Catalysis</i> , 2022, 12, 3063-3082.	5.5	8
4	Ammonia-Assisted Light Alkane Anti-coke Reforming on Isolated ReO _x Sites in Zeolite. <i>ACS Catalysis</i> , 2022, 12, 3165-3172.	5.5	6
5	Revealing the interplay between "intelligent behavior" and surface reconstruction of non-precious metal doped SrTiO ₃ catalysts during methane combustion. <i>Catalysis Today</i> , 2022, , .	2.2	5
6	Single Atoms Anchored in Hexagonal Boron Nitride for Propane Dehydrogenation from First Principles. <i>ChemCatChem</i> , 2022, 14, .	1.8	6
7	Multiple Promotional Effects of Vanadium Oxide on Boron Nitride for Oxidative Dehydrogenation of Propane. <i>Jacs Au</i> , 2022, 2, 1096-1104.	3.6	20
8	Manganese Catalyzed Partial Oxidation of Light Alkanes. <i>ACS Catalysis</i> , 2022, 12, 5356-5370.	5.5	9
9	Surface engineering of MXenes for energy and environmental applications. <i>Journal of Materials Chemistry A</i> , 2022, 10, 10265-10296.	5.2	41
10	MoS ₂ nanosheet integrated electrodes with engineered 1T-2H phases and defects for efficient hydrogen production in practical PEM electrolysis. <i>Applied Catalysis B: Environmental</i> , 2022, 313, 121458.	10.8	33
11	Defect-Regulated Frustrated-Lewis-Pair Behavior of Boron Nitride in Ambient Pressure Hydrogen Activation. <i>Journal of the American Chemical Society</i> , 2022, 144, 10688-10693.	6.6	17
12	CO ₂ methanation reaction pathways over unpromoted and NaNO ₃ -promoted Ru/Al ₂ O ₃ catalysts. <i>Catalysis Science and Technology</i> , 2022, 12, 4637-4652.	2.1	7
13	Defect Engineering of Ceria Nanocrystals for Enhanced Catalysis via a High-Entropy Oxide Strategy. <i>ACS Central Science</i> , 2022, 8, 1081-1090.	5.3	25
14	Measuring and directing charge transfer in heterogenous catalysts. <i>Nature Communications</i> , 2022, 13, .	5.8	19
15	Enhanced performance of (Tj ETQq1 1 0.784314 rgBT /Overlock 10 T) with indium surfactant. <i>Materials Letters</i> , 2022, 324, 132675.	1.3	0
16	Popularity-Based and Version-Aware Caching Scheme at Edge Servers for Multi-Version VoD Systems. <i>IEEE Transactions on Circuits and Systems for Video Technology</i> , 2021, 31, 1234-1248.	5.6	9
17	Vacancy engineering of the nickel-based catalysts for enhanced CO ₂ methanation. <i>Applied Catalysis B: Environmental</i> , 2021, 282, 119561.	10.8	100
18	All-solid-state Z-scheme BiVO ₄ ~Bi ₆ O ₆ (OH) ₃ (NO ₃) ₃ heterostructure with prolonging electron-hole lifetime for enhanced photocatalytic hydrogen and oxygen evolution. <i>Journal of Materials Science and Technology</i> , 2021, 77, 117-125.	5.6	16

#	ARTICLE	IF	CITATIONS
19	<i>In Situ</i> Strong Metal-Support Interaction (SMSI) Affects Catalytic Alcohol Conversion. ACS Catalysis, 2021, 11, 1938-1945.	5.5	50
20	A tailored multi-functional catalyst for ultra-efficient styrene production under a cyclic redox scheme. Nature Communications, 2021, 12, 1329.	5.8	35
21	Oxidative Dehydrogenation of Propane to Propylene with Soft Oxidants via Heterogeneous Catalysis. ACS Catalysis, 2021, 11, 2182-2234.	5.5	97
22	Machine Learning Method Reveals Hidden Strong Metal-Support Interaction in Microscopy Datasets. Small Methods, 2021, 5, 2100035.	4.6	13
23	Elucidating the origin of selective dehydrogenation of propane on γ -alumina under H ₂ S treatment and co-feed. Journal of Catalysis, 2021, 394, 142-156.	3.1	21
24	Deep Learning Accelerated Determination of Hydride Locations in Metal Nanoclusters. Angewandte Chemie - International Edition, 2021, 60, 12289-12292.	7.2	23
25	Deep Learning Accelerated Determination of Hydride Locations in Metal Nanoclusters. Angewandte Chemie, 2021, 133, 12397-12400.	1.6	0
26	Ultrathin platinum nanowire based electrodes for high-efficiency hydrogen generation in practical electrolyzer cells. Chemical Engineering Journal, 2021, 410, 128333.	6.6	40
27	New Insights into the Bulk and Surface Defect Structures of Ceria Nanocrystals from Neutron Scattering Study. Chemistry of Materials, 2021, 33, 3959-3970.	3.2	24
28	Inelastic Neutron Scattering Observation of Plasma-Promoted Nitrogen Reduction Intermediates on Ni/ γ -Al ₂ O ₃ . ACS Energy Letters, 2021, 6, 2048-2053.	8.8	20
29	On the Structural Transformation of Ni/BaH ₂ During a N ₂ -H ₂ Chemical Looping Process for Ammonia Synthesis: A Joint In Situ Inelastic Neutron Scattering and First-Principles Simulation Study. Topics in Catalysis, 2021, 64, 685-692.	1.3	11
30	Elucidating the Mechanism of Ambient-Temperature Aldol Condensation of Acetaldehyde on Ceria. ACS Catalysis, 2021, 11, 8621-8634.	5.5	14
31	Photoinduced Strong Metal-Support Interaction for Enhanced Catalysis. Journal of the American Chemical Society, 2021, 143, 8521-8526.	6.6	85
32	Isolated Metal Sites in Cu-Zn-Y/Beta for Direct and Selective Butene-Rich C ₃₊ Olefin Formation from Ethanol. ACS Catalysis, 2021, 11, 9885-9897.	5.5	24
33	Preface to Special Issue on Neutron Scattering for Catalysis. Topics in Catalysis, 2021, 64, 591-592.	1.3	1
34	A Review on the Impact of SO ₂ on the Oxidation of NO, Hydrocarbons, and CO in Diesel Emission Control Catalysis. ACS Catalysis, 2021, 11, 12446-12468.	5.5	36
35	In situ spectroscopic insights into the redox and acid-base properties of ceria catalysts. Chinese Journal of Catalysis, 2021, 42, 2122-2140.	6.9	12
36	Atomically Dispersed Tin-Modified γ -alumina for Selective Propane Dehydrogenation under H ₂ S Co-feed. ACS Catalysis, 2021, 11, 13472-13482.	5.5	8

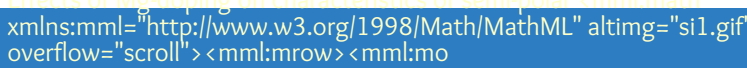
#	ARTICLE	IF	CITATIONS
37	Implementation and Analysis of Hybrid DRAM PUFs on FPGA. , 2021, , .		0
38	Understanding the conversion of ethanol to propene on In ₂ O ₃ from first principles. <i>Catalysis Today</i> , 2020, 350, 19-24.	2.2	16
39	A new trick for an old support: Stabilizing gold single atoms on LaFeO ₃ perovskite. <i>Applied Catalysis B: Environmental</i> , 2020, 261, 118178.	10.8	31
40	Pd-promoted WO ₃ -ZrO ₂ for low temperature NO _x storage. <i>Applied Catalysis B: Environmental</i> , 2020, 264, 118499.	10.8	30
41	Solvent-free and one-pot synthesis of ultramicroporous carbons with ultrahigh nitrogen contents for sulfur dioxide capture. <i>Chemical Engineering Journal</i> , 2020, 391, 123579.	6.6	32
42	Solar-driven efficient methane catalytic oxidation over epitaxial ZnO/La _{0.8} Sr _{0.2} CoO ₃ heterojunctions. <i>Applied Catalysis B: Environmental</i> , 2020, 265, 118469.	10.8	44
43	Alcohol-Induced Low-Temperature Blockage of Supported-Metal Catalysts for Enhanced Catalysis. <i>ACS Catalysis</i> , 2020, 10, 8515-8523.	5.5	18
44	Hydrogen in Nanocatalysis. <i>Journal of Physical Chemistry Letters</i> , 2020, 11, 7049-7057.	2.1	18
45	Descriptors for Hydrogen Evolution on Single Atom Catalysts in Nitrogen-Doped Graphene. <i>Journal of Physical Chemistry C</i> , 2020, 124, 19571-19578.	1.5	75
46	H ₂ O-prompted CO ₂ capture on metal silicates <i>in situ</i> generated from SBA-15. <i>RSC Advances</i> , 2020, 10, 28731-28740.	1.7	3
47	Stable Surface Terminations of a Perovskite Oxyhydride from First-Principles. <i>Journal of Physical Chemistry C</i> , 2020, 124, 18557-18563.	1.5	5
48	A Principle for Highly Active Metal Oxide Catalysts via NaCl-Based Solid Solution. <i>Chem</i> , 2020, 6, 1723-1741.	5.8	30
49	Construction of 2D BiVO ₄ ~CdS~Ti ₃ C ₂ T _x Heterostructures for Enhanced Photo~redox Activities. <i>ChemCatChem</i> , 2020, 12, 3496-3503.	1.8	25
50	Activation and surface reactions of CO and H ₂ on ZnO powders and nanoplates under CO hydrogenation reaction conditions. <i>Journal of Energy Chemistry</i> , 2020, 50, 351-357.	7.1	22
51	PdPt-TiO ₂ nanowires: correlating composition, electronic effects and O-vacancies with activities towards water splitting and oxygen reduction. <i>Applied Catalysis B: Environmental</i> , 2020, 277, 119177.	10.8	36
52	Harnessing strong metal~support interactions via a reverse route. <i>Nature Communications</i> , 2020, 11, 3042.	5.8	84
53	Titelbild: Radical Chemistry and Reaction Mechanisms of Propane Oxidative Dehydrogenation over Hexagonal Boron Nitride Catalysts (<i>Angew. Chem.</i> 21/2020). <i>Angewandte Chemie</i> , 2020, 132, 8045-8045.	1.6	0
54	Radical Chemistry and Reaction Mechanisms of Propane Oxidative Dehydrogenation over Hexagonal Boron Nitride Catalysts. <i>Angewandte Chemie - International Edition</i> , 2020, 59, 8042-8046.	7.2	83

#	ARTICLE	IF	CITATIONS
55	Radical Chemistry and Reaction Mechanisms of Propane Oxidative Dehydrogenation over Hexagonal Boron Nitride Catalysts. <i>Angewandte Chemie</i> , 2020, 132, 8119-8123.	1.6	11
56	The interplay between surface facet and reconstruction on isopropanol conversion over SrTiO ₃ nanocrystals. <i>Journal of Catalysis</i> , 2020, 384, 49-60.	3.1	19
57	Perovskite-supported Pt single atoms for methane activation. <i>Journal of Materials Chemistry A</i> , 2020, 8, 4362-4368.	5.2	31
58	World Trade Wars: Scenario Calculations of Consequences. <i>Herald of the Russian Academy of Sciences</i> , 2020, 90, 88-97.	0.2	4
59	Effects of Surface Terminations of 2D Bi ₂ WO ₆ on Photocatalytic Hydrogen Evolution from Water Splitting. <i>ACS Applied Materials & Interfaces</i> , 2020, 12, 20067-20074.	4.0	78
60	Discriminating the Role of Surface Hydride and Hydroxyl for Acetylene Semihydrogenation over Ceria through <i>In Situ</i> Neutron and Infrared Spectroscopy. <i>ACS Catalysis</i> , 2020, 10, 5278-5287.	5.5	70
61	Nature of Reactive Hydrogen for Ammonia Synthesis over a Ru/C12A7 Electride Catalyst. <i>Journal of the American Chemical Society</i> , 2020, 142, 7655-7667.	6.6	59
62	A review of the interactions between ceria and H ₂ and the applications to selective hydrogenation of alkynes. <i>Chinese Journal of Catalysis</i> , 2020, 41, 901-914.	6.9	40
63	Mechanistic Understanding of Catalytic Conversion of Ethanol to 1-Butene over 2D-Pillared MFI Zeolite. <i>Journal of Physical Chemistry C</i> , 2020, 124, 28437-28447.	1.5	9
64	All-solid-state supercapacitors from natural lignin-based composite film by laser direct writing. <i>Applied Physics Letters</i> , 2019, 115, .	1.5	46
65	An overview of photocatalysis facilitated by 2D heterojunctions. <i>Nanotechnology</i> , 2019, 30, 502002.	1.3	66
66	Crucial influential factor on background electron concentration in semi-polar (111) AlGaInN/GaN heterostructure. <i>Optik</i> , 2019, 192, 162978.	1.4	3
67	plane AlGaIn epi-layers. <i>Superlattices and Microstructures</i> , 2019, 125, 338-342. Promoting Pt catalysis for CO oxidation via the Mott-Schottky effect. <i>Nanoscale</i> , 2019, 11, 18568-18574.	2.8	13
68	Effects of indium surfactant and MgN intermediate layers on surface morphology and crystalline quality of nonpolar a-plane AlGaIn epi-layers. <i>Optik</i> , 2019, 192, 162978.	1.4	6
69	Effect of Hydrogen-Induced Metallization on Chemisorption. <i>Journal of Physical Chemistry C</i> , 2019, 123, 15171-15175.	1.5	3
70	Enhanced hole concentration and improved surface morphology for nonpolar a-plane p-type AlGaIn/GaN superlattices grown with indium-surfactant. <i>Superlattices and Microstructures</i> , 2019, 130, 396-400.	1.4	10
71	Monolayer Ti ₃ C ₂ Tx as an Effective Co-catalyst for Enhanced Photocatalytic Hydrogen Production over TiO ₂ . <i>ACS Applied Energy Materials</i> , 2019, 2, 4640-4651.	2.5	177
72	Surface Reconstructions of Metal Oxides and the Consequences on Catalytic Chemistry. <i>ACS Catalysis</i> , 2019, 9, 5692-5707.	5.5	127

#	ARTICLE	IF	CITATIONS
73	Interaction of SO ₂ with ZnO Nanoshapes: Impact of Surface Polarity. Journal of Physical Chemistry C, 2019, 123, 11772-11780.	1.5	21
74	Elucidation of the Reaction Mechanism for High-Temperature Water Gas Shift over an Industrial-Type Copper-Chromium-Iron Oxide Catalyst. Journal of the American Chemical Society, 2019, 141, 7990-7999.	6.6	60
75	In situ spectroscopy-guided engineering of rhodium single-atom catalysts for CO oxidation. Nature Communications, 2019, 10, 1330.	5.8	177
76	Effects of Sodium and Tungsten Promoters on Mg ₆ MnO ₈ -Based Core-Shell Redox Catalysts for Chemical Looping Oxidative Dehydrogenation of Ethane. ACS Catalysis, 2019, 9, 3174-3186.	5.5	52
77	Impact of Surface Composition of SrTiO ₃ Catalysts for Oxidative Coupling of Methane. ChemCatChem, 2019, 11, 2107-2117.	1.8	41
78	Fabrication of a Pillared ZSM-5 Framework for Shape Selectivity of Ethane Dehydroaromatization. Industrial & Engineering Chemistry Research, 2019, 58, 7094-7106.	1.8	19
79	2D/2D heterojunction of Ti ₃ C ₂ /g-C ₃ N ₄ nanosheets for enhanced photocatalytic hydrogen evolution. Nanoscale, 2019, 11, 8138-8149.	2.8	289
80	Work-in-Progress: Version-Aware Video Caching Strategy for Multi-version VoD Systems. , 2019, , .		1
81	Study of NH ₃ flow duty-ratio in pulsed-flow epitaxial growth of non-polar a-plane Al _{0.34} Ga _{0.66} N films. Materials Science in Semiconductor Processing, 2019, 90, 219-224.	1.9	7
82	Neutron Scattering Investigations of Hydride Species in Heterogeneous Catalysis. ChemSusChem, 2019, 12, 5-5.	3.6	0
83	Neutron Scattering Investigations of Hydride Species in Heterogeneous Catalysis. ChemSusChem, 2019, 12, 93-103.	3.6	29
84	Optimizing the structural configuration of FePt-FeOx nanoparticles at the atomic scale by tuning the post-synthetic conditions. Nano Energy, 2019, 55, 441-446.	8.2	10
85	High Internal Quantum Efficiency of Nonpolar a-Plane AlGaIn-Based Multiple Quantum Wells Grown on r-Plane Sapphire Substrate. ACS Photonics, 2018, 5, 1903-1906.	3.2	33
86	CO oxidation over ceria supported Au ₂₂ nanoclusters: Shape effect of the support. Chinese Chemical Letters, 2018, 29, 795-799.	4.8	45
87	Role of Interfaces in Two-Dimensional Photocatalyst for Water Splitting. ACS Catalysis, 2018, 8, 2253-2276.	5.5	773
88	Interface Engineering of Earth-Abundant Transition Metals Using Boron Nitride for Selective Electroreduction of CO ₂ . ACS Applied Materials & Interfaces, 2018, 10, 6694-6700.	4.0	52
89	Enhanced hole concentration in nonpolar a-plane p-AlGaIn film with multiple-step rapid thermal annealing technique. Journal Physics D: Applied Physics, 2018, 51, 095101.	1.3	5
90	One-Step Synthesis of Nb ₂ O ₅ /C/Nb ₂ C (MXene) Composites and Their Use as Photocatalysts for Hydrogen Evolution. ChemSusChem, 2018, 11, 688-699.	3.6	315

#	ARTICLE	IF	CITATIONS
91	Fabrication of Au ₂₅ (SG) ₁₈ â€”ZIFâ€”8 Nanocomposites: A Facile Strategy to Position Au ₂₅ (SG) ₁₈ Nanoclusters Inside and Outside ZIFâ€”8. <i>Advanced Materials</i> , 2018, 30, 1704576.	11.1	129
92	Effects of TiO ₂ in Low Temperature Propylene Epoxidation Using Gold Catalysts. <i>Journal of Physical Chemistry C</i> , 2018, 122, 1688-1698.	1.5	37
93	Acidâ€”base catalysis over perovskites: a review. <i>Journal of Materials Chemistry A</i> , 2018, 6, 2877-2894.	5.2	101
94	A physical catalyst for the electrolysis of nitrogen to ammonia. <i>Science Advances</i> , 2018, 4, e1700336.	4.7	264
95	Molecular structure and sour gas surface chemistry of supported K ₂ O/WO ₃ /Al ₂ O ₃ catalysts. <i>Applied Catalysis B: Environmental</i> , 2018, 232, 146-154.	10.8	19
96	Understanding Methanol Coupling on SrTiO ₃ from First Principles. <i>Journal of Physical Chemistry C</i> , 2018, 122, 7210-7216.	1.5	2
97	Stronger-than-Pt hydrogen adsorption in a Au ₂₂ nanocluster for the hydrogen evolution reaction. <i>Journal of Materials Chemistry A</i> , 2018, 6, 7532-7537.	5.2	63
98	Catalysis on Singly Dispersed Rh Atoms Anchored on an Inert Support. <i>ACS Catalysis</i> , 2018, 8, 110-121.	5.5	81
99	Characterizations of weakly sharp solutions for a variational inequality with a pseudomonotone mapping. <i>European Journal of Operational Research</i> , 2018, 265, 448-453.	3.5	8
100	Shape Effect Undermined by Surface Reconstruction: Ethanol Dehydrogenation over Shape-Controlled SrTiO ₃ Nanocrystals. <i>ACS Catalysis</i> , 2018, 8, 555-565.	5.5	59
101	Acetic Acid/Propionic Acid Conversion on Metal Doped Molybdenum Carbide Catalyst Beads for Catalytic Hot Gas Filtration. <i>Catalysts</i> , 2018, 8, 643.	1.6	8
102	Understanding the Impact of Surface Reconstruction of Perovskite Catalysts on CH ₄ Activation and Combustion. <i>ACS Catalysis</i> , 2018, 8, 10306-10315.	5.5	50
103	DMOF-1 as a Representative MOF for SO ₂ Adsorption in Both Humid and Dry Conditions. <i>Journal of Physical Chemistry C</i> , 2018, 122, 23493-23500.	1.5	51
104	New Bonding Model of Radical Adsorbate on Lattice Oxygen of Perovskites. <i>Journal of Physical Chemistry Letters</i> , 2018, 9, 6321-6325.	2.1	37
105	Study of dual nitridation processes in growth of non-polar a-plane AlGaN epi-layers. <i>Materials Letters</i> , 2018, 227, 108-111.	1.3	8
106	Effects of indium surfactant on growth and characteristics of $\hat{A}(112\hat{A}^{-2})$ plane AlGaN-based multiple quantum wells. <i>Optical Materials Express</i> , 2018, 8, 24.	1.6	9
107	An extend RBAC model for privacy protection in HIS. , 2018, , .		0
108	First Principles Insight into H ₂ Activation and Hydride Species on TiO ₂ Surfaces. <i>Journal of Physical Chemistry C</i> , 2018, 122, 20323-20328.	1.5	44

#	ARTICLE	IF	CITATIONS
109	Exploring perovskites for methane activation from first principles. <i>Catalysis Science and Technology</i> , 2018, 8, 702-709.	2.1	35
110	Epitaxial growth of semi-polar (11 $\bar{2}$ 2) plane AlGa _N epilayers on a-plane (10 $\bar{1}$ 0) sapphire substrates. <i>Physica Status Solidi (A) Applications and Materials Science</i> , 2017, 214, 1600802.	0.8	8
111	Aminopolymer functionalization of boron nitride nanosheets for highly efficient capture of carbon dioxide. <i>Journal of Materials Chemistry A</i> , 2017, 5, 16241-16248.	5.2	67
112	Toward the Design of a Hierarchical Perovskite Support: Ultra-Sintering-Resistant Gold Nanocatalysts for CO Oxidation. <i>ACS Catalysis</i> , 2017, 7, 3388-3393.	5.5	40
113	Effect of metal oxides modification on CO ₂ adsorption performance over mesoporous carbon. <i>Microporous and Mesoporous Materials</i> , 2017, 249, 34-41.	2.2	47
114	Influence of nitridation process on characteristics of N-polar AlGa _N films grown by MOCVD. <i>Materials Science in Semiconductor Processing</i> , 2017, 64, 147-151.	1.9	8
115	Epitaxial growth and characterization of nonpolar a-plane AlGa _N films with MgN/AlGa _N insertion layers. <i>Applied Physics Express</i> , 2017, 10, 045503.	1.1	5
116	Single Pd Atoms on γ -Al ₂ O ₃ (010) Surface do not Catalyze NO Oxidation. <i>Scientific Reports</i> , 2017, 7, 560.	1.6	19
117	Metallic Hydrogen in Atomically Precise Gold Nanoclusters. <i>Chemistry of Materials</i> , 2017, 29, 4840-4847.	3.2	70
118	High-performance stacked in-plane supercapacitors and supercapacitor array fabricated by femtosecond laser 3D direct writing on polyimide sheets. <i>Electrochimica Acta</i> , 2017, 241, 153-161.	2.6	93
119	Quantitative Analysis of the Morphology of {101} and {001} Faceted Anatase TiO ₂ Nanocrystals and Its Implication on Photocatalytic Activity. <i>Chemistry of Materials</i> , 2017, 29, 5591-5604.	3.2	65
120	Controlling Reaction Selectivity through the Surface Termination of Perovskite Catalysts. <i>Angewandte Chemie</i> , 2017, 129, 9952-9956.	1.6	19
121	Controlling Reaction Selectivity through the Surface Termination of Perovskite Catalysts. <i>Angewandte Chemie - International Edition</i> , 2017, 56, 9820-9824.	7.2	47
122	Enhanced visible light photocatalytic water reduction from a g-C ₃ N ₄ /SrTa ₂ O ₆ heterojunction. <i>Applied Catalysis B: Environmental</i> , 2017, 217, 448-458.	10.8	58
123	High hole concentration in nonpolar a-plane p-AlGa _N films with Mg-delta doping technique. <i>Superlattices and Microstructures</i> , 2017, 109, 880-885.	1.4	10
124	Controlling interfacial properties in supported metal oxide catalysts through metal-organic framework templating. <i>Journal of Materials Chemistry A</i> , 2017, 5, 13565-13572.	5.2	15
125	Taming interfacial electronic properties of platinum nanoparticles on vacancy-abundant boron nitride nanosheets for enhanced catalysis. <i>Nature Communications</i> , 2017, 8, 15291.	5.8	200
126	Acid-Base Reactivity of Perovskite Catalysts Probed via Conversion of 2-Propanol over Titanates and Zirconates. <i>ACS Catalysis</i> , 2017, 7, 4423-4434.	5.5	81

#	ARTICLE	IF	CITATIONS
127	Selective conversion of bio-derived ethanol to renewable BTX over Ga-ZSM-5. <i>Green Chemistry</i> , 2017, 19, 4344-4352.	4.6	57
128	Catalytic Dehydration of Biomass Derived 1-Propanol to Propene over M-ZSM-5 (M = H, V, Cu, or Zn). <i>Industrial & Engineering Chemistry Research</i> , 2017, 56, 4302-4308.	1.8	15
129	Improved crystalline quality of N-polar GaN epitaxial layers grown with reformed flow-rate-modulation technology. <i>Japanese Journal of Applied Physics</i> , 2017, 56, 015501.	0.8	5
130	Defects reduction in a-plane AlGaIn epi-layers grown on r-plane sapphire substrates by metal organic chemical vapor deposition. <i>Applied Physics Express</i> , 2017, 10, 011002.	1.1	25
131	Nature of Active Sites and Surface Intermediates during SCR of NO with NH ₃ by Supported V ₂ O ₅ /WO ₃ /TiO ₂ Catalysts. <i>Journal of the American Chemical Society</i> , 2017, 139, 15624-15627.	6.6	266
132	Effect of Surface Structure of TiO ₂ Nanoparticles on CO ₂ Adsorption and SO ₂ Resistance. <i>ACS Sustainable Chemistry and Engineering</i> , 2017, 5, 9295-9306. Effects of Mg doping on characteristics of semi-polar AlGaN	3.2	49
133			

#	ARTICLE	IF	CITATIONS
145	Synergistic Effects of Water and SO ₂ on Degradation of MIL-125 in the Presence of Acid Gases. <i>Journal of Physical Chemistry C</i> , 2016, 120, 27230-27240.	1.5	79
146	Effects of Si-doping on structural, electrical, and optical properties of polar and non-polar AlGaIn epi-layers. <i>Superlattices and Microstructures</i> , 2016, 96, 1-7.	1.4	13
147	Influence of catalyst synthesis method on selective catalytic reduction (SCR) of NO by NH ₃ with V ₂ O ₅ -WO ₃ /TiO ₂ catalysts. <i>Applied Catalysis B: Environmental</i> , 2016, 193, 141-150.	10.8	136
148	In-Plane Heterojunctions Enable Multiphase Two-Dimensional (2D) MoS ₂ Nanosheets As Efficient Photocatalysts for Hydrogen Evolution from Water Reduction. <i>ACS Catalysis</i> , 2016, 6, 6723-6729.	5.5	116
149	High Selectivity Electrochemical Conversion of CO ₂ to Ethanol using a Copper Nanoparticle/N-doped Graphene Electrode. <i>ChemistrySelect</i> , 2016, 1, 6055-6061.	0.7	251
150	Effects of growth temperature on characteristics of Mg-delta-doped p-AlInGaIn epi-layers. <i>Superlattices and Microstructures</i> , 2016, 98, 181-186.	1.4	4
151	Diphosphine-Protected Au ₂₂ Nanoclusters on Oxide Supports Are Active for Gas-Phase Catalysis without Ligand Removal. <i>Nano Letters</i> , 2016, 16, 6560-6567.	4.5	88
152	Towards ALD thin film stabilized single-atom Pd ₁ catalysts. <i>Nanoscale</i> , 2016, 8, 15348-15356.	2.8	98
153	Promotional Effects of In on Non-Oxidative Methane Transformation Over Mo-ZSM-5. <i>Catalysis Letters</i> , 2016, 146, 1903-1909.	1.4	10
154	Extraction, antioxidant and antibacterial activities of Broussonetia papyrifera fruits polysaccharides. <i>International Journal of Biological Macromolecules</i> , 2016, 92, 116-124.	3.6	92
155	Cu-Enhanced Surface Defects and Lattice Mobility of Pr-CeO ₂ Mixed Oxides. <i>Journal of Physical Chemistry C</i> , 2016, 120, 27996-28008.	1.5	9
156	Atomic Surface Structures of Oxide Nanoparticles with Well-defined Shapes. <i>Microscopy and Microanalysis</i> , 2016, 22, 360-361.	0.2	0
157	Titania Composites with 2% Transition Metal Carbides as Photocatalysts for Hydrogen Production under Visible Light Irradiation. <i>ChemSusChem</i> , 2016, 9, 1490-1497.	3.6	253
158	Effects of Si-doping on structural and electrical characteristics of polar, semi-polar, and non-polar AlGaIn epi-layers. <i>Materials Science in Semiconductor Processing</i> , 2016, 42, 344-348.	1.9	15
159	Fundamental Understanding of the Interaction of Acid Gases with CeO ₂ : From Surface Science to Practical Catalysis. <i>Industrial & Engineering Chemistry Research</i> , 2016, 55, 3909-3919.	1.8	26
160	High-rate in-plane micro-supercapacitors scribed onto photo paper using in situ femtolaser-reduced graphene oxide/Au nanoparticle microelectrodes. <i>Energy and Environmental Science</i> , 2016, 9, 1458-1467.	15.6	202
161	Selective catalytic reduction of NO by NH ₃ with WO ₃ -TiO ₂ catalysts: Influence of catalyst synthesis method. <i>Applied Catalysis B: Environmental</i> , 2016, 188, 123-133.	10.8	51
162	In situ studies of surface of NiFe ₂ O ₄ catalyst during complete oxidation of methane. <i>Surface Science</i> , 2016, 648, 156-162.	0.8	35

#	ARTICLE	IF	CITATIONS
163	Oxidative dehydrogenation of isobutane over vanadia catalysts supported by titania nanoshapes. <i>Catalysis Today</i> , 2016, 263, 84-90.	2.2	17
164	Role of defects and metal coordination on adsorption of acid gases in MOFs and metal oxides: An in situ IR spectroscopic study. <i>Microporous and Mesoporous Materials</i> , 2016, 227, 65-75.	2.2	29
165	Low temperature propane oxidation over Co ₃ O ₄ based nano-array catalysts: Ni dopant effect, reaction mechanism and structural stability. <i>Applied Catalysis B: Environmental</i> , 2016, 180, 150-160.	10.8	174
166	Characterization of weakly sharp solutions of a variational inequality by its primal gap function. <i>Optimization Letters</i> , 2016, 10, 563-576.	0.9	16
167	Effect of Dopants on the Adsorption of Carbon Dioxide on Ceria Surfaces. <i>ChemSusChem</i> , 2015, 8, 3651-3660.	3.6	61
168	Spectroscopic Investigation of Surface-Dependent Acid-Base Property of Ceria Nanoshapes. <i>Journal of Physical Chemistry C</i> , 2015, 119, 7340-7350.	1.5	156
169	Application Analysis on Large-Scale Computation for Social and Economic Systems: Application Case from China. , 2015, , .		2
170	Highly selective adsorption of ethylene over ethane in a MOF featuring the combination of open metal site and π -complexation. <i>Chemical Communications</i> , 2015, 51, 2714-2717.	2.2	151
171	Understanding complete oxidation of methane on spinel oxides at a molecular level. <i>Nature Communications</i> , 2015, 6, 7798.	5.8	237
172	Adhesion and Atomic Structures of Gold on Ceria Nanostructures: The Role of Surface Structure and Oxidation State of Ceria Supports. <i>Nano Letters</i> , 2015, 15, 5375-5381.	4.5	98
173	Constructing Hierarchical Interfaces: TiO ₂ -Supported PtFe@FeO Nanowires for Room Temperature CO Oxidation. <i>Journal of the American Chemical Society</i> , 2015, 137, 10156-10159.	6.6	86
174	Robust Ag nanoplate ink for flexible electronics packaging. <i>Nanoscale</i> , 2015, 7, 7368-7377.	2.8	71
175	The Characterization and Structure-Dependent Catalysis of Ceria with Well-Defined Facets. , 2015, , 71-97.		5
176	Role Of CO ₂ As a Soft Oxidant For Dehydrogenation of Ethylbenzene to Styrene over a High-Surface-Area Ceria Catalyst. <i>ACS Catalysis</i> , 2015, 5, 6426-6435.	5.5	90
177	Mesoporous MnCeO _x solid solutions for low temperature and selective oxidation of hydrocarbons. <i>Nature Communications</i> , 2015, 6, 8446.	5.8	241
178	Visible-light-driven Bi ₂ O ₃ /WO ₃ composites with enhanced photocatalytic activity. <i>RSC Advances</i> , 2015, 5, 91094-91102.	1.7	54
179	Surface Structure Dependence of SO ₂ Interaction with Ceria Nanocrystals with Well-Defined Surface Facets. <i>Journal of Physical Chemistry C</i> , 2015, 119, 28895-28905.	1.5	26
180	Aromatic- π -hydroxyl interaction of an alpha-aryl ether lignin model-compound on SBA-15, present at pyrolysis temperatures. <i>Physical Chemistry Chemical Physics</i> , 2014, 16, 24188-24193.	1.3	18

#	ARTICLE	IF	CITATIONS
181	Infrared Spectroscopic Insights into the Role of the Support in Heterogeneous Gold Catalysis. RSC Catalysis Series, 2014, , 512-532.	0.1	0
182	Multi-wavelength Raman spectroscopy study of supported vanadia catalysts: Structure identification and quantification. Chinese Journal of Catalysis, 2014, 35, 1591-1608.	6.9	12
183	Three-Phase Catalytic System of H ₂ O, Ionic Liquid, and VOPO ₄ ·SiO ₂ Solid Acid for Conversion of Fructose to 5-Hydroxymethylfurfural. ChemSusChem, 2014, 7, 1703-1709.	3.6	28
184	Imaging the Atomic Surface Structures of CeO ₂ Nanoparticles. Nano Letters, 2014, 14, 191-196.	4.5	183
185	Origin of Active Oxygen in a Ternary CuO _x /Co ₃ O ₄ ·CeO ₂ Catalyst for CO Oxidation. Journal of Physical Chemistry C, 2014, 118, 27870-27877.	1.5	50
186	Growth and Electrochemical Characterization of Carbon Nanospire Thin Film Electrodes. Journal of the Electrochemical Society, 2014, 161, H558-H563.	1.3	24
187	Thiolate Ligands as a Double-Edged Sword for CO Oxidation on CeO ₂ Supported Au ₂₅ (SCH ₂ CH ₂ Ph) ₁₈ Nanoclusters. Journal of the American Chemical Society, 2014, 136, 6111-6122.	6.6	245
188	Introduction of π -Complexation into Porous Aromatic Framework for Highly Selective Adsorption of Ethylene over Ethane. Journal of the American Chemical Society, 2014, 136, 8654-8660.	6.6	383
189	Adsorption and Reaction of Acetaldehyde on Shape-Controlled CeO ₂ Nanocrystals: Elucidation of Structure-Function Relationships. ACS Catalysis, 2014, 4, 2437-2448.	5.5	128
190	Surface structure dependence of selective oxidation of ethanol on faceted CeO ₂ nanocrystals. Journal of Catalysis, 2013, 306, 164-176.	3.1	95
191	CO Oxidation on Supported Single Pt Atoms: Experimental and ab Initio Density Functional Studies of CO Interaction with Pt Atom on γ -Al ₂ O ₃ (010) Surface. Journal of the American Chemical Society, 2013, 135, 12634-12645.	6.6	535
192	Shape-Controlled Ceria-Based Nanostructures for Catalysis Applications. ChemSusChem, 2013, 6, 1821-1833.	3.6	176
193	Inelastic neutron scattering, Raman and DFT investigations of the adsorption of phenanthrenequinone on onion-like carbon. Carbon, 2013, 52, 150-157.	5.4	14
194	Anomalous High Ionic Conductivity of Nanoporous β -Li ₃ PS ₄ . Journal of the American Chemical Society, 2013, 135, 975-978.	6.6	709
195	Utilizing Surface Enhanced Raman Spectroscopy for the Study of Interfacial Phenomena: Probing Interactions on an Alumina Surface. ACS Symposium Series, 2013, , 101-114.	0.5	0
196	Oxygen-Functionalized Few-Layer Graphene Sheets as Active Catalysts for Oxidative Dehydrogenation Reactions. ChemSusChem, 2013, 6, 840-846.	3.6	61
197	Oxygen-Functionalized Few-Layer Graphene Sheets as Active Catalysts for Oxidative Dehydrogenation Reactions. ChemSusChem, 2013, 6, 732-732.	3.6	1
198	Heterometal Incorporation in Metal-Exchanged Zeolites Enables Low-Temperature Catalytic Activity of NO _x Reduction. Journal of Physical Chemistry C, 2012, 116, 23322-23331.	1.5	48

#	ARTICLE	IF	CITATIONS
199	Galvanic synthesis of bi-modal porous metal nanostructures using aluminum nanoparticle templates. <i>Materials Letters</i> , 2012, 88, 143-147.	1.3	19
200	A Raman Spectroscopic Study of the Speciation of Vanadia Supported on Ceria Nanocrystals with Defined Surface Planes. <i>ChemCatChem</i> , 2012, 4, 1653-1661.	1.8	40
201	In situ growth synthesis of heterostructured LnPO ₄ @SiO ₂ (Ln = La, Ce, and Eu) mesoporous materials as supports for small gold particles used in catalytic CO oxidation. <i>Journal of Materials Chemistry</i> , 2012, 22, 25227.	6.7	18
202	Support Shape Effect in Metal Oxide Catalysis: Ceria-Nanoshape-Supported Vanadia Catalysts for Oxidative Dehydrogenation of Isobutane. <i>Journal of Physical Chemistry Letters</i> , 2012, 3, 1517-1522.	2.1	72
203	Probing the Surface Sites of CeO ₂ Nanocrystals with Well-Defined Surface Planes via Methanol Adsorption and Desorption. <i>ACS Catalysis</i> , 2012, 2, 2224-2234.	5.5	165
204	On the structure dependence of CO oxidation over CeO ₂ nanocrystals with well-defined surface planes. <i>Journal of Catalysis</i> , 2012, 285, 61-73.	3.1	553
205	Synthesis of silica supported AuCu nanoparticle catalysts and the effects of pretreatment conditions for the CO oxidation reaction. <i>Physical Chemistry Chemical Physics</i> , 2011, 13, 2571.	1.3	92
206	<i>In Situ</i> High Temperature Surface Enhanced Raman Spectroscopy for the Study of Interface Phenomena: Probing a Solid Acid on Alumina. <i>Journal of Physical Chemistry C</i> , 2011, 115, 9068-9073.	1.5	19
207	Reply to Comment on "Multiwavelength Raman Spectroscopic Study of Silica-Supported Vanadium Oxide Catalysts". <i>Journal of Physical Chemistry C</i> , 2011, 115, 10925-10928.	1.5	2
208	Preparation and Characterization of PdFe Nanoleaves as Electrocatalysts for Oxygen Reduction Reaction. <i>Chemistry of Materials</i> , 2011, 23, 1570-1577.	3.2	106
209	CO oxidation on phosphate-supported Au catalysts: Effect of support reducibility on surface reactions. <i>Journal of Catalysis</i> , 2011, 278, 133-142.	3.1	42
210	Structure of Vanadium Oxide Supported on Ceria by Multiwavelength Raman Spectroscopy. <i>Journal of Physical Chemistry C</i> , 2011, 115, 25368-25378.	1.5	91
211	Ultra-thin PtFe-nanowires as durable electrocatalysts for fuel cells. <i>Nanotechnology</i> , 2011, 22, 015602.	1.3	50
212	Raman study of Fano interference in <i>p</i> -type doped silicon. <i>Journal of Raman Spectroscopy</i> , 2010, 41, 1759-1764.	1.2	49
213	Probing Defect Sites on CeO ₂ Nanocrystals with Well-Defined Surface Planes by Raman Spectroscopy and O ₂ Adsorption. <i>Langmuir</i> , 2010, 26, 16595-16606.	1.6	889
214	Multiwavelength Raman Spectroscopic Study of Silica-Supported Vanadium Oxide Catalysts. <i>Journal of Physical Chemistry C</i> , 2010, 114, 412-422.	1.5	80
215	CO oxidation on Au/FePO ₄ catalyst: Reaction pathways and nature of Au sites. <i>Journal of Catalysis</i> , 2009, 266, 98-105.	3.1	56
216	Investigation of the selective sites on graphitic carbons for oxidative dehydrogenation of isobutane. <i>Journal of Catalysis</i> , 2009, 267, 158-166.	3.1	42

#	ARTICLE	IF	CITATIONS
217	The role of surface vanadia species in butane dehydrogenation over VO _x /Al ₂ O ₃ . <i>Catalysis Today</i> , 2009, 142, 143-151.	2.2	35
218	Low-Temperature Solution-Phase Synthesis of NiAu Alloy Nanoparticles via Butyllithium Reduction: Influences of Synthesis Details and Application As the Precursor to Active Au-NiO/SiO ₂ Catalysts through Proper Pretreatment. <i>Journal of Physical Chemistry C</i> , 2009, 113, 5758-5765.	1.5	50
219	DRIFTS-QMS Study of Room Temperature CO Oxidation on Au/SiO ₂ Catalyst: Nature and Role of Different Au Species. <i>Journal of Physical Chemistry C</i> , 2009, 113, 3726-3734.	1.5	79
220	Self-Assembly of Metal Oxide Nanoparticles into Hierarchically Patterned Porous Architectures Using Ionic Liquid/Oil Emulsions. <i>Langmuir</i> , 2009, 25, 7229-7233.	1.6	22
221	In Situ Phase Separation of NiAu Alloy Nanoparticles for Preparing Highly Active Au/NiO CO Oxidation Catalysts. <i>ChemPhysChem</i> , 2008, 9, 2475-2479.	1.0	91
222	Gâteaux differentiability of the dual gap function of a variational inequality. <i>European Journal of Operational Research</i> , 2008, 190, 328-344.	3.5	7
223	The convexity of the solution set of a pseudoconvex inequality. <i>Nonlinear Analysis: Theory, Methods & Applications</i> , 2008, 69, 1666-1674.	0.6	3
224	Oxygen-assisted reduction of Au species on Au/SiO ₂ catalyst in room temperature CO oxidation. <i>Chemical Communications</i> , 2008, , 3308.	2.2	29
225	Raman Spectroscopic Study of V ₂ O ₅ /Al ₂ O ₃ Catalysts: Quantification of Surface Vanadia Species and Their Structure Reduced by Hydrogen. <i>Journal of Physical Chemistry C</i> , 2007, 111, 16460-16469.	1.5	53
226	A comparison of catalyst deactivation of vanadia catalysts used for alkane dehydrogenation. <i>Chemical Engineering Journal</i> , 2006, 120, 127-132.	6.6	21
227	Influence of absorption on quantitative analysis in Raman spectroscopy. <i>Catalysis Today</i> , 2006, 113, 40-47.	2.2	36
228	UV Raman spectroscopic studies of V ₂ O ₅ /Al ₂ O ₃ catalysts in butane dehydrogenation. <i>Journal of Catalysis</i> , 2006, 237, 220-229.	3.1	60
229	The synergic effect between Mo species and acid sites in Mo/HMCM-22 catalysts for methane aromatization. <i>Physical Chemistry Chemical Physics</i> , 2005, 7, 3102.	1.3	33
230	On the Structure of Vanadium Oxide Supported on Aluminas: UV and Visible Raman Spectroscopy, UV-Visible Diffuse Reflectance Spectroscopy, and Temperature-Programmed Reduction Studies. <i>Journal of Physical Chemistry B</i> , 2005, 109, 2793-2800.	1.2	167
231	Vibrational spectra of alumina- and silica-supported vanadia revisited: An experimental and theoretical model catalyst study. <i>Journal of Catalysis</i> , 2004, 226, 88-100.	3.1	258
232	Dibenzothiophene hydrodesulfurization activity and surface sites of silica-supported MoP, Ni ₂ P, and NiMoP catalysts. <i>Journal of Catalysis</i> , 2004, 228, 298-310.	3.1	154
233	In situ IR Spectroscopic Studies on Molybdenum Nitride Catalysts: Active Sites and Surface Reactions. <i>ChemInform</i> , 2004, 35, no.	0.1	0
234	On the surface sites of MoP/SiO ₂ catalyst under sulfiding conditions: IR spectroscopy and catalytic reactivity studies. <i>Journal of Catalysis</i> , 2004, 222, 41-52.	3.1	64

#	ARTICLE	IF	CITATIONS
235	The reaction route and active site of catalytic decomposition of hydrazine over molybdenum nitride catalyst. <i>Journal of Catalysis</i> , 2004, 224, 473-478.	3.1	100
236	Adsorption and reaction of thiophene and H ₂ S on Mo ₂ C/Al ₂ O ₃ catalyst studied by in situ FT-IR spectroscopy. <i>Physical Chemistry Chemical Physics</i> , 2004, 6, 5596.	1.3	10
237	An IR study on the surface passivation of Mo ₂ C/Al ₂ O ₃ catalyst with O ₂ , H ₂ O and CO ₂ . <i>Physical Chemistry Chemical Physics</i> , 2004, 6, 5603.	1.3	33
238	Weak Sharp Solutions of Variational Inequalities in Hilbert Spaces. <i>SIAM Journal on Optimization</i> , 2004, 14, 1011-1027.	1.2	38
239	Title is missing!. <i>Catalysis Surveys From Asia</i> , 2003, 7, 103-119.	1.0	11
240	Carbon Monoxide Adsorption on Molybdenum Phosphides: A Fourier Transform Infrared Spectroscopic and Density Functional Theory Studies. <i>Journal of Physical Chemistry B</i> , 2003, 107, 13698-13702.	1.2	26
241	In Situ FT-IR Spectroscopic Studies of CO Adsorption on Fresh Mo ₂ C/Al ₂ O ₃ Catalyst. <i>Journal of Physical Chemistry B</i> , 2003, 107, 7088-7094.	1.2	71
242	Microcalorimetric and IR spectroscopic studies of CO adsorption on molybdenum nitride catalysts. <i>Physical Chemistry Chemical Physics</i> , 2003, 5, 1703-1707.	1.3	5
243	FT-IR Spectroscopic Studies of Thiophene Adsorption and Reactions on Mo ₂ N/Al ₂ O ₃ Catalysts. <i>Journal of Physical Chemistry B</i> , 2002, 106, 979-987.	1.2	50
244	Title is missing!. <i>Catalysis Letters</i> , 2002, 79, 21-25.	1.4	55
245	Selective Hydrogenation of 1,3-Butadiene on Molybdenum Nitride Catalyst: Identification of the Adsorbed Hydrocarbonaceous Species. <i>Studies in Surface Science and Catalysis</i> , 2001, 138, 445-452.	1.5	2
246	A novel reaction on a Mo ₂ N/Al ₂ O ₃ catalyst: low-temperature isomerization of but-1-ene. <i>Chemical Communications</i> , 2001, , 701-702.	2.2	13
247	Low-Temperature Isomerization of 1-Butene on Mo ₂ N/Al ₂ O ₃ Catalyst Studied by in Situ FT-IR Spectroscopy. <i>Journal of Physical Chemistry B</i> , 2001, 105, 9183-9190.	1.2	23
248	Epoxidation of cyclohexene on Ti/SiO ₂ catalysts prepared by chemical grafting TiCl ₄ on deboronated silica xerogel. <i>Journal of Molecular Catalysis A</i> , 2001, 172, 219-225.	4.8	10
249	Sulfur effect on Mo ₂ N/Al ₂ O ₃ catalyst studied by in situ FT-IR spectroscopy. <i>Studies in Surface Science and Catalysis</i> , 2000, 130, 2819-2824.	1.5	4
250	Sulfur Effect on Mo ₂ N/Al ₂ O ₃ Catalyst Studied by in Situ FT-IR Spectroscopy. <i>Journal of Catalysis</i> , 2000, 194, 23-32.	3.1	23
251	An IR Study on Selective Hydrogenation of 1,3-Butadiene on Transition Metal Nitrides: A 1,3-Butadiene and 1-Butene Adsorption on Mo ₂ N/Al ₂ O ₃ Catalyst. <i>Journal of Physical Chemistry B</i> , 2000, 104, 12275-12281.	1.2	34
252	A Region-Interactive Retrieval Model Based on IRM Algorithm. , 0, , .		0

#	ARTICLE	IF	CITATIONS
253	Resonance Raman Spectroscopy of γ -Al ₂ O ₃ -Supported Vanadium Oxide Catalysts as an Illustrative Example. , 0, , 177-194.		2